






A Low-mass Stellar-debris Stream Associated with a Globular Cluster Pair in the Halo

Zhen Yuan¹ , Jiang Chang^{2,3}, Timothy C. Beers⁴ , and Yang Huang⁵ ¹ Key Laboratory for Research in Galaxies and Cosmology, Shanghai Astronomical Observatory, Chinese Academy of Sciences, 80 Nandan Road, Shanghai 200030, People's Republic of China; sala.yuan@gmail.com² Key Lab of Optical Astronomy, National Astronomical Observatories, CAS, 20A Datun Road, Chaoyang District, 100012 Beijing, People's Republic of China³ Purple Mountain Observatory, CAS, No.8 Yuanhua Road, Qixia District, Nanjing 210034, People's Republic of China⁴ Department of Physics and JINA Center for the Evolution of the Elements (JINA-CEE), University of Notre Dame, Notre Dame, IN 46556, USA⁵ South-Western Institute For Astronomy Research, Yunnan University, Kunming 650500, People's Republic of China

Received 2020 June 1; revised 2020 July 2; accepted 2020 July 9; published 2020 July 29

Abstract

There are expected to be physical relationships between the globular clusters (GCs) and stellar substructures in the Milky Way, not all of which have yet been found. We search for such substructures from a combined halo sample of SDSS blue horizontal-branch and SDSS+LAMOST RR Lyrae stars, cross-matched with astrometric information from Gaia DR2. This is a sample of old stars which are also excellent tracers of structures, ideal for searching for ancient relics in the outer stellar halo. By applying the neural-network-based method STARGO to the full 4D dynamical space of our sample, we rediscover the Sagittarius Stream, and find the debris of the Gaia-Enceladus-Sausage and the Sequoia events in the outer halo, as well as their linkages with several GCs. Most importantly, we find a new, low-mass, debris stream associated with a pair of GCs (NGC 5024 and NGC 5053), which we dub LMS-1. This stream has a very polar orbit, and occupies a region between 10 to 20 kpc from the Galactic center. NGC 5024 (M53), the more massive of the associated GC pair, is very likely the nuclear star cluster of a now-disrupted dwarf galaxy progenitor, based on the results from N -body simulations.

Unified Astronomy Thesaurus concepts: Milky Way stellar halo (1060); Globular star clusters (656)

1. Introduction

According to the Λ CDM cosmological model, the Milky Way (MW) has grown to its current size through mergers with numerous neighboring dwarf galaxies. Thanks to the advent of the Gaia mission (Gaia Collaboration et al. 2018), the stellar debris from relatively massive merger events such as the Gaia-Enceladus-Sausage (GES; Belokurov et al. 2018; Haywood et al. 2018; Helmi et al. 2018; Myeong et al. 2018a) and the Sequoia (Seq; Myeong et al. 2019) have been identified in the inner stellar halo. In the outer stellar halo, the full 6D panoramic portrait of the Sagittarius (Sgr) stream has been obtained for the first time (Antoja et al. 2020; Ibata et al. 2020; Ramos et al. 2020). These well-studied substructures and streams are the fossils from dwarf galaxies with dark matter halo masses of 10^{10} – $10^{11}M_{\odot}$. The relics from less-massive dwarf galaxies engulfed by the MW are far more difficult to identify. However, based on the hierarchical paradigm of galaxy formation, the majority of the building blocks of the MW are expected to be small ($\lesssim 10^9M_{\odot}$). The identification of numerous minor mergers is thus essential for unraveling the complete assembly history of the MW.

Also importantly, low-mass dwarf galaxies have relatively short star formation histories, and thus can provide direct records of the high-redshift ($z \sim 5$) universe, the epoch when globular clusters (GCs) were also formed. These clusters later fell into the MW as their host galaxies were disrupted, thus we would expect MW GCs to be connected to halo substructures. Indeed, such associations have been seen in M31 from recent photometric studies (see, e.g., Mackey et al. 2010, 2019; Huxor et al. 2011). Similar relationships are less obvious in our Galaxy, as their detection relies on spectroscopic data for numerous individual stars. The few substructures in the MW known to be associated with GCs, the Sgr stream, the GES, and Seq, are all expected to have originated from massive accreted

dwarf progenitors. Although GCs likely also populated less-massive progenitors, as has been found in nearby dwarf galaxies (see, e.g., Georgiev et al. 2010), their dwarf progenitors are expected to have been fully disrupted in the outer halo before sinking deep into the Galactic potential.

In order to identify the substructures associated with GCs stripped from lower-mass progenitors, we employ a sample of halo stars comprising two types of old stars, blue horizontal-branch (BHB) and RR Lyrae (RRL) stars. Such stars are not only representatives of the ancient halo, but are also excellent tracers of structure, owing to their precise distance estimates. Previous studies of substructure identification in dynamical space are limited to the inner-halo region, due to the lack of good distance estimates for more distant stars. The large range of distances of this halo sample, with an uncertainty as low as 5% (based on photometry only), allows us to identify dynamically tagged groups (DTGs) in the outer halo. In Section 2, we combine the SDSS BHB and SDSS+LAMOST RRL catalogs, and cross-match with Gaia DR2 (Lindgren et al. 2018), yielding ~ 7600 stars with full 6D phase-space information. The group-identification approach is discussed in detail in Section 3. The DTGs with GC associations are presented in Section 4, including both existing and newly identified substructures. A summary and brief conclusions are provided in Section 5.

2. Data

We combine a previous SDSS BHB catalog (Xue et al. 2008) with the recently released SDSS+LAMOST RRL catalog (Liu et al. 2020) to create a halo sample of 7640 stars that have full 6D kinematic information available. For BHB stars, line-of-sight velocities are derived from the SEGUE Stellar Parameter Pipeline (Lee et al. 2008a, 2008b), with uncertainties of 5 km s^{-1} to 15 km s^{-1} (Xue et al. 2008). The

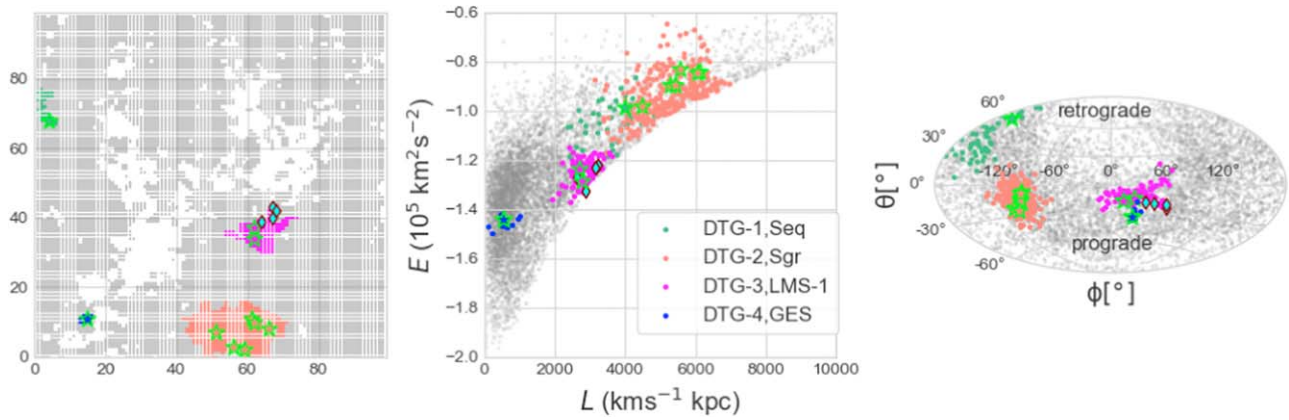


Figure 1. Dynamically tagged groups (DTGs) and associated globular clusters (GCs) on the trained map (left panel), and in the input space (E , L , θ , ϕ) in the right two panels, where the latter two angles characterize the directions of orbital poles in Galactocentric coordinates. The gray circles in the right two panels represent the halo sample used in this study. The four DTGs are shown with different colors (green, salmon, magenta, blue), and form separated clumps in the input space. The GCs associated with each DTG are plotted by lime star symbols filled by the same color as the group color, and are well within the corresponding clump. The four outliers stars are marked by cyan diamonds, which sit at the edge of DTG-3 on the neuron map and in the projection of orbital poles (see Section 4.2 for details).

velocities of RRLs are taken from Liu et al. (2020), which utilizes empirical templates to fit velocity curves of multiple measurements from the LAMOST (Deng et al. 2012; Zhao et al. 2012) and the SDSS/SEGUE (Yanny et al. 2009) surveys. Depending on the number of measurements, the velocity precision varies from 5 km s^{-1} to 15 km s^{-1} . The distance estimates for both types of stars are obtained from multi-band photometry with mean uncertainties of about 5% (Xue et al. 2008, 2014; Liu et al. 2020). We then cross-match the halo sample with Gaia DR2 (Lindegren et al. 2018). Given the magnitude range of the sample ($G \sim 17\text{--}19$), the errors of the proper motion measurements range from 0.13 to 0.60 mas yr^{-1} . Combining with the distance uncertainty of 5%, the typical transverse velocity uncertainty is about 15 km s^{-1} for the majority of stars in the sample, located 10 to 20 kpc from the Sun. This is equivalent to the uncertainty of the line-of-sight velocities. The resulting errors in the orbital parameters and other dynamical properties are sufficiently small to enable detection of significant groups in dynamical space. For the MW GCs, we employ the catalog from Harris (2010), with proper motions determined by Vasiliev (2019a).

3. Method

We apply the neural-network-based clustering method STARGO (Yuan et al. 2018) to search for substructures that are clustered in the 4D space of orbital energy and angular momentum, both of which are approximately conserved, even in non-spherical potentials (e.g., Helmi & de Zeeuw 2000). The gravitational potential of McMillan (2017) is used to derive dynamical parameters with AGAMA (Vasiliev 2019b). As in the previous work from Yuan et al. (2019, 2020), we use (E , L , θ , ϕ) as the input space, where the latter two angular parameters characterize directions of the orbital poles, and are defined as

$$\theta = \arccos(L_z/L), \quad \phi = \arctan(L_x/L_y). \quad (1)$$

We use a 100×100 neuron network, and follow a similar recipe as Yuan et al. (2020) to identify dynamical groups. Each grid point of the neuron map hosts one neuron, as shown in the left panel of Figure 1, which has an initially randomized 4D weight vector. For a given input vector, the neuron that has the weight vector closest to it is defined as its best-matching unit

(BMU). Each neuron updates its weight vectors to come closer to the input vector in the 4D space; the learning effectiveness depends on its distance to the BMU on the 2D map. The weight vectors of the neurons close to the BMU will be assimilated into the input vector more efficiently compared to those neurons located farther away. The final result of the learning process is a converged map, after a sufficient number of iterations. This process preserves the structure of the input data, and projects it onto a 2D map.

The learning results can be revealed by differences in the weight vectors between adjacent neurons, which are defined as a 100×100 u -matrix. In the left panel of Figure 1, the gray-colored neurons have the top 20% u values, denoting the lowest 20% similarities between neighbors. These neurons form gray boundaries, and separate the others into isolated islands (see the white patches in the left panel). Compared to the boundary neurons, those in islands have more similar weight vectors, and thus correspond to stars clustered in dynamical space. The idea of group identification is to find the islands isolated by the gray boundaries as we scan the threshold (u_{thr}) that defines the boundary. We check the significance and contamination of neuron groups at each threshold value when they appear as isolated islands. In this way, we are able to systematically identify all the significant groups of stars clustered in the input space. In Figure 1, we show all of the four groups identified in this work, for three different values of u_{thr} . They are plotted by different colors on the neuron map shown in the left panel. The corresponding star groups form separate clusters in the input space shown in the right two panels.

Evaluation of the significance and contamination of each detected group is implemented as a post process. We first draw a Monte Carlo sample of 10,000 mock stars, based on the probability density function, in each dimension of the input space. Then we connect each mock star with its BMU on the trained neuron map, and obtain the probability (p) of a mock star being associated to a detected group \mathcal{G} of n members. The significance of \mathcal{G} can be quantified by the binomial probability of detecting more than n stars from the halo sample of \mathcal{N} stars. The contamination can be derived as $p/(n/\mathcal{N})$. We consider \mathcal{G} as valid only if the significance is larger than 5σ and the contamination rate is less than 20%. For each DTG, the valid members are re-verified by their probabilities ($p \geq 20\%$) of

Table 1
Properties of DTGs and Associated GCs

u_{thr}	\mathcal{G}	n_{BHB}	n_{RRL}	\mathcal{F}_c	Conf.	$\langle [\text{Fe}/\text{H}] \rangle$	$\sigma_{[\text{Fe}/\text{H}]}$ (dex)	Substructure	Globular Clusters
$u_1(60\text{th})$	DTG-1	29	12	14%	48%	-2.05 ± 0.09	0.58 ± 0.07	Seq	NGC 6101 (100%)
$u_2(45\text{th})$	DTG-2	116	136	6%	63%	-1.87 ± 0.02	0.31 ± 0.02	Sgr	Whiting 1 (78%), M 54 (100%), Terzan 7 (100%), Arp 2 (99%), Terzan 8 (100%), Pal 12 (50%)
$u_3(20\text{th})$	DTG-3	75	20	9%	73%	-2.09 ± 0.04	0.25 ± 0.03	LMS-1	NGC 5024 (100%), NGC 5053 (100%)
	DTG-4	3	5	0%	39%	$-1.84^{+0.24}_{-0.25}$	$0.65^{+0.21}_{-0.16}$	GES	NGC 6864 (M 75) (62%)

being associated to the same group, after taking the observational uncertainties into account. The confidence of each DTG is derived as the average probability of its valid member stars being associated to it.

After validation of the detected groups, we check if any valid group is associated to known MW GCs. This is done by generating 1000 realizations for each GC, according to its observational uncertainties in 6D kinematics. As done for the mapping of mock stars, we connect each realization of a given GC with its BMU on the neuron map. The confidence level of the association between a GC and a DTG is quantified by the probability of the mock GC sample being associated with the same DTG. This value is used to compare the associations of different GCs with their DTGs.

4. Results

In this work, we focus on the substructures that are dynamically associated with MW GCs. Although numerous valid DTGs could be identified from the trained neuron map, only those having strong associations with GCs are analyzed in this work. In total, we identify four DTGs at three different values of u_{thr} . The details of these groups are summarized in Table 1, where n_{BHB} and n_{RRL} denote the number of group members from the SDSS BHB and SDSS+LAMOST RRL samples, respectively. The contamination fraction, \mathcal{F}_c , and confidence level for each DTG are listed, as well as its mean and dispersion of $[\text{Fe}/\text{H}]$. The assigned substructures and associated GCs are shown in the last two columns. Since our halo sample is mainly populated by stars with $[\text{Fe}/\text{H}] \lesssim -1.5$, all of the identified DTGs have very low mean metallicities ($[\text{Fe}/\text{H}] \approx -1.8$ to -2.0). After taking into account the observational error of each group member star, the intrinsic dispersions of $[\text{Fe}/\text{H}]$ of these DTGs are in the range of 0.25–0.65 dex, which excludes the possibility of their progenitors being GCs. Figure 1 clearly shows that all the DTGs stand out from the gray background of the halo sample, and form separate clumps in the input space of (E, L) and (θ, ϕ) . We note that, except for DTG-1 (green), which has a retrograde orbit with positive θ , the other three groups, DTG-2 (salmon), DTG-3 (magenta), and DTG-4 (blue), all have prograde orbits with negative θ . The GCs associated with each DTG are embedded well within its individual clump, shown as lime star symbols filled by the same colors as their DTGs. The confidence level of each association, derived in the same way as that of each member star, is provided in parentheses following the GC name in the last column of Table 1.

Figure 2 shows the location of the DTGs and their associated GCs in different dynamical-space visualizations, color-coded as in Figure 1. We differentiate the BHB members from the RRL members by filling the former with blue colors. The left panel of Figure 2 shows the projected action-space map.

DTG-1 clearly occupies the corner of retrograde orbits, and DTG-4 is situated in the region representing radial orbits. DTG-2 and DTG-3 have fairly polar orbits, and significantly overlap with each other in this projection; note that DTG-2 has higher orbital energy than DTG-3, which makes them clearly separable in the (E, L_z) space shown in the right panel. DTG-1 has slightly lower energy than DTG-2, but they have distinguishable distributions of L_z . Among all the groups, DTG-4 has the lowest energy, as well as the lowest rotational motion. Utilizing these features of orbital properties, we analyze and assign an origin to each group below.

4.1. Existing Substructures

The first valid group with a GC association is DTG-1, identified at $u_{\text{thr}} = u_{60\%}$. This is the only retrograde group found in this work, which consists of 29 BHB and 12 RRL stars. A great number of streams and substructures with retrograde motions have been reported by several studies (Grillmair & Dionatos 2006; Malhan et al. 2018, 2019; Myeong et al. 2018b; Price-Whelan & Bonaca 2018; Koppelman et al. 2019; Matsuno et al. 2019; Yuan et al. 2020). These groups are contributed to by at least one substantial merger event that took place at an early epoch, Seq (Myeong et al. 2019), which also brought in several retrograde GCs. The distribution of DTG-1 in the action-space map and (E, L_z) overlaps perfectly with that of the Seq groups found in the inner halo with $d \lesssim 10$ kpc (Matsuno et al. 2019; Myeong et al. 2019; Yuan et al. 2020). The stars in DTG-1 reside at 10 kpc to 40 kpc from the Sun, but most of them have pericenter distances $\lesssim 10$ kpc, similar to the Seq relic, which is also consistent with their relatively low orbital energy $E \sim -10^5$ to $-1.2 \times 10^5 \text{ km}^2 \text{ s}^{-2}$. This implies that DTG-1 comes from an early accreted dwarf galaxy, possibly the same one as Seq. DTG-1 is very likely part of the Seq debris that currently occupies the outer halo.

By applying the approach discussed in Section 3, we find that DTG-1 is dynamically associated with NGC 6101, which is also categorized as a Seq GC according to two different studies (Massari et al. 2019; Myeong et al. 2019). NGC 6101 has a mass of $\sim 10^5 M_\odot$ and low metallicity, $[\text{Fe}/\text{H}] = -1.98$ (Harris 2010), consistent with the picture that it was born in the early star formation epochs of a classical dwarf galaxy, and accreted to the MW during the merger. We integrate the orbit of NGC 6101 in forward and backward directions for about three orbital periods (1.5 Gyr, $T_{\text{orb}} \approx 0.5$ Gyr), shown in the first panel of Figure 3. Although the GC is currently situated in the South, its orbit comes across the Galactic plane and traverses most of the stellar members above the plane.

The largest group among the four is DTG-2, identified at $u = u_{45\%}$, which has 116 BHB and 136 RRL members, covering a large heliocentric distance range from 5 to 50 kpc.

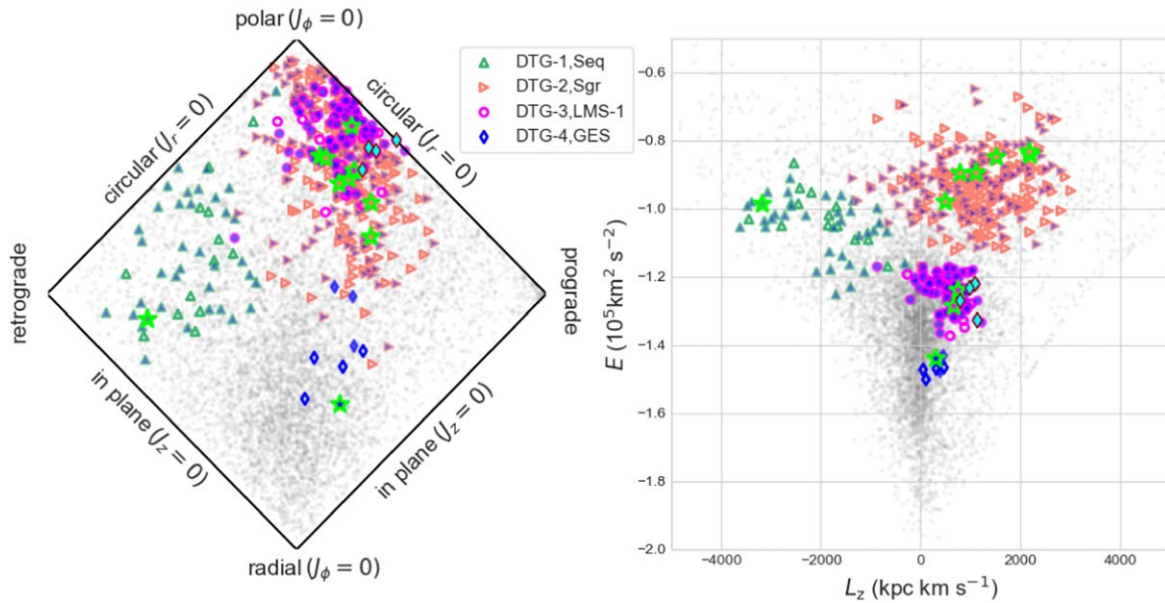


Figure 2. DTGs and their associated GCs in dynamical space. Left: the projected action-space map. The x -axis is (J_ϕ/J_{tot}) , and the y -axis is $(J_z - J_r)/J_{\text{tot}}$, where $J_{\text{tot}} = J_z + J_r + |J_\phi|$. Right: the space of orbital energy vs. the z -component of angular momentum. The gray circles represent the halo sample. The four DTGs are plotted by different colors and symbols, and the BHB members are filled by blue colors. The GCs are plotted by lime star symbols filled by the same color as the associated groups. DTG-1 (green upper triangles) has a very retrograde orbit, and DTG-4 (blue diamonds) exhibits prominent radial motion. Both DTG-2 (salmon right triangles) and DTG-3 (magenta circles) have fairly polar orbits, whereas the former has higher energy.

The on-sky projection of DTG-2 in equatorial coordinates reveals it as the Sgr stream (see the second panel of Figure 3). We find that six GCs (Whiting 1, M 54, Terzan 7, Arp 2, Terzan 8, and Pal 12) are associated to DTG-2, all of which have been confirmed to be associated with the Sgr stream by previous studies (see, e.g., Law & Majewski 2010; Sohn et al. 2018; Bellazzini et al. 2020). Note that the association of Pal 12 has the lowest confidence level (50%), among all the GC associations identified in this work.

Another group with distinctive orbital features is DTG-4, comprising three BHB member and five RRL stars, located between 7 to 15 kpc from the Galactic center, with a prominent radial motion and high orbital eccentricity, $e \sim 0.7$. The orbital energy is fairly low, $E \sim -1.45 \times 10^5 \text{ km}^2 \text{ s}^{-2}$, characterizing it as an inner-halo substructure. All of these properties suggest that DTG-4 very likely comes from the GES, which is an early, massive radial-merger event (Belokurov et al. 2018; Helmi et al. 2018). Its associated GC, M75 (NGC 6864), is also identified as a GES globular cluster by both Myeong et al. (2018a) and Massari et al. (2019). We plot DTG-4 and its associated GC, in Galactic coordinates, in the bottom panel of Figure 3. Six members at $l \sim 30^\circ$ – 60° are located in the region of the Northern Hercules Aquila Cloud (HAC), and NGC 6864 is in the Southern HAC (Belokurov et al. 2007; Simion et al. 2014). The other two member at $l \approx -60^\circ$ are in the area of the Virgo Over-Density (VOD), which has been shown to share the same origin as the HAC (see Simion et al. 2019 and references therein).

4.2. The Polar Stream LMS-1

There is only one group, DTG-3, that cannot be assigned to any existing substructures. DTG-3 has 75 BHB and 20 RRL members, shown as the magenta group in Figures 1 and 2. It has intermediate orbital energy ($E \sim -1.4 \times 10^5$ to $-1.2 \times 10^5 \text{ km}^2 \text{ s}^{-2}$), between DTG-4, representing the GES debris in the inner halo, and DTG-2, confirmed as the Sgr Stream in the outer halo. The stellar members

of DTG-3 have Galactocentric distances $r \sim 10$ – 25 kpc and pericentric distances $r_p \lesssim 15$ kpc. As for the Sgr stream identified in this work, its stellar members have $r \sim 15$ – 45 kpc, and $r_p \lesssim 30$ kpc. This indicates that DTG-3 is situated closer to the Galactic center than the Sgr stream, consistent with its lower orbital energy. DTG-3 has an average orbital inclination angle of 80° , which is more polar than the Sgr Stream (76°) identified in this work. We plot the on-sky projection of DTG-3, in Galactic coordinates, shown as the magenta group in the third panel of Figure 3. It spans a wide region on the sky, with a coverage of more than 100° in l , while maintaining a relatively coherent structure, like the Sgr stream shown in the second panel. Most of the stream members are populated in the North, with three members found in the South, owing to the limited sky coverage of both the SDSS and LAMOST surveys. We name this substructure as the low-mass stellar-debris stream (LMS-1), because it is a wide debris-stream similar to the Sgr stream, but is made up of much fewer members.

The two associated GCs are not only embedded in LMS-1 in dynamical space (see Figures 1 and 2), but also in configuration space (see the on-sky projection in Figure 3). The two GCs are currently located in the distance range of the LMS-1 members, at $r \approx 18$ kpc, close to their apocenters ($r_a \approx 20$ kpc). They have pericentric distances $r_p \approx 10$ kpc, similar to the LMS-1 members. The separation between these two GCs is 500 pc, but their velocity difference is $\sim 200 \text{ km s}^{-1}$, which makes them a unique and intriguing pair. NGC 5024 (M53), in the rank of massive GCs in the MW, has a mass of $\sim 5 \times 10^5 M_\odot$ (Harris 2010), and $[\text{Fe}/\text{H}] = -2.07$ (Boberg et al. 2016), which is much more massive than its companion NGC 5053, with a mass of $\sim 5 \times 10^4 M_\odot$ (Baumgardt 2017), and $[\text{Fe}/\text{H}] = -2.45$ (Boberg et al. 2015). We emphasize that, although the two GCs are very close together, they are not bound to each other. However, it is very unlikely that they just happen to be passing by one another. Chun et al. (2010) showed that this GC pair is surrounded by a complex stellar envelope, using deep

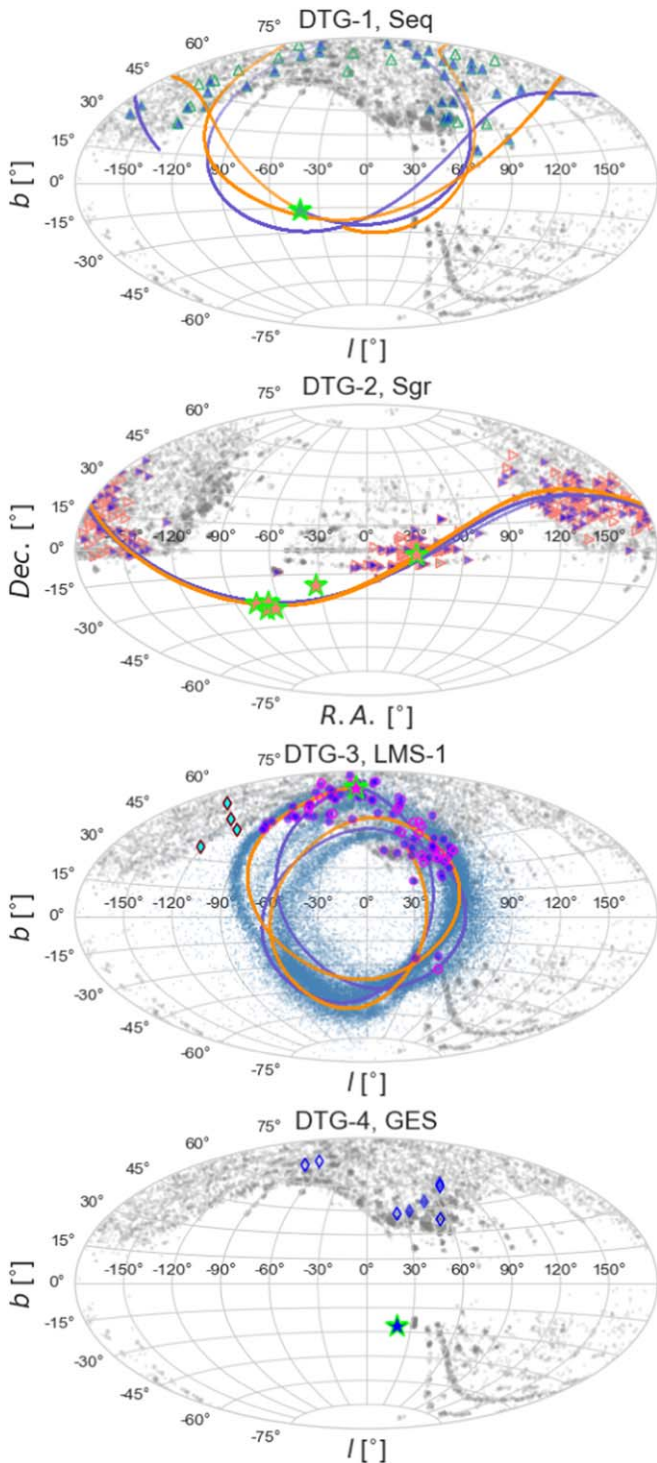


Figure 3. On-sky projection of four DTGs and their associated GCs, superposed on the halo sample, plotted in the same way as Figure 2. First panel: DTG-1 (Seq; green upper triangles) and NGC 6101 in Galactic coordinates. The forward-integrated orbit (purple) and backward orbit (orange) of the GC traverse the group members, which are all populated in the North. Second panel: DTG-2 (the Sgr stream; salmon right triangles), in equatorial coordinates, and the six associated GCs, Whiting 1 (R.A. $\approx 30^\circ$), NGC 6715 (M 54), Terzan 7, Arp 2, Terzan 8, and Pal 12. Third panel: DTG-3 (LMS-1; magenta circles) and its associated pair of GCs, in Galactic coordinates. The steel-blue circles denote the simulated stream on the orbit of NGC 5024 (purple: forward; orange: backward) with eight apocentric passages, coincident with the stream members in both hemispheres. The four outliers at $l \sim -120^\circ$ are highlighted by cyan diamonds. Fourth panel: DTG-4 (GES; blue diamonds) and NGC 6864, in Galactic coordinates, which are located in the region of the Virgo Over-Density and Hercules Aquila Cloud.

photometric data from MegaCam. Ngeow et al. (2020) claimed there are no extra-tidal RRLs associated with them within $\sim 8 \text{ deg}^2$. Massari et al. (2019) attributed these two GCs to the Helmi Stream. In this work, we show that this GC pair is embedded in a wide stream, suggesting they were stripped from the same parent dwarf galaxy. This also naturally leads to the plausible scenario that the relatively massive GC (NGC 5024) could be the core of the dwarf galaxy progenitor of both the stellar stream and the GCs. To verify this possibility, we trace the orbit of NGC 5024 for about three periods of time ($T_{\text{orb}} \approx 0.32 \text{ Gyr}$) in both backward (orange line) and forward (blue line) directions, as shown in Figure 3. The trajectory of NGC 5024 traverses the majority of the stream members located in the North, with four outliers at $l \approx -120^\circ$ (cyan diamonds), and perfectly matches with the three Southern members as well. These outlier stars, sitting at the edge of the distribution of the orbital poles of LMS-1 (see the right panel of Figure 1), are possibly the result of orbital precession. Although the orbit of NGC 5053 is very similar to that of NGC 5024, given their large mass difference, the nuclear star cluster of the dwarf galaxy progenitor of LMS-1 was very likely NGC 5024, whereas NGC 5053 was off-center, and stripped at a different epoch. This could explain why the two GCs are coincidentally almost at the same place now, but not in a dynamically bound system. While this Letter was being reviewed, Naidu et al. (2020) reported the discovery of a new substructure, “Wukong,” which has similar dynamical properties as LMS-1. There are three GCs (NGC 5024, NGC 5053, and ESO 280-SC06) attributed to “Wukong” in their studies, whereas only the first two are identified as dynamically associated to LMS-1 in this work.

All the DTGs identified in this work are fairly metal-poor, because the halo sample used is a combination of two types of old stars. However, it is noteworthy that the mean metallicity of LMS-1 ($\langle [\text{Fe}/\text{H}] \rangle = -2.09$) is similar to that of the Seq DTG ($\langle [\text{Fe}/\text{H}] \rangle = -2.05$), and is slightly lower than those of the Sgr stream and the GES groups ($\langle [\text{Fe}/\text{H}] \rangle \approx -1.8$), implying that the progenitor dwarf galaxies of both LMS-1 and Seq are less massive than the other two. The number of the LMS-1 members is about one-third of the number of the Sgr members in our sample of BHB and RRL stars. This is in-line with the number of GCs associated with these two streams: the Sgr stream has six GCs and LMS-1 has two. This again indicates that the dwarf galaxy progenitor of LMS-1 is smaller than the Sgr dwarf, but still massive enough to host two GCs. This might be the reason that LMS-1 was not discovered by previous photometric studies, as it has much lower surface brightness compared with the Sgr stream. We have simulated LMS-1 using a dwarf satellite with a total mass of $2 \times 10^9 M_\odot$, given that the Sgr progenitor mass is $\sim 10^{10} M_\odot$. The initial condition of the satellite is derived by rewinding the orbit of NGC 5024 for eight orbital periods. The orbital information at its first apocentric passage is recorded as the initial condition of the dwarf satellite. We then let it evolve in the MW potential for about eight orbital periods ($\sim 2.4 \text{ Gyr}$). It is fully disrupted now, and has strewn stream members across the Galactic plane, shown as the blue scatter in the third panel of Figure 3. As can be seen, the simulated stream agrees well with the integrated orbit of NGC 5024, and can fully cover the footprint of LMS-1, as also shown, in Galactic coordinates, in Figure 4.

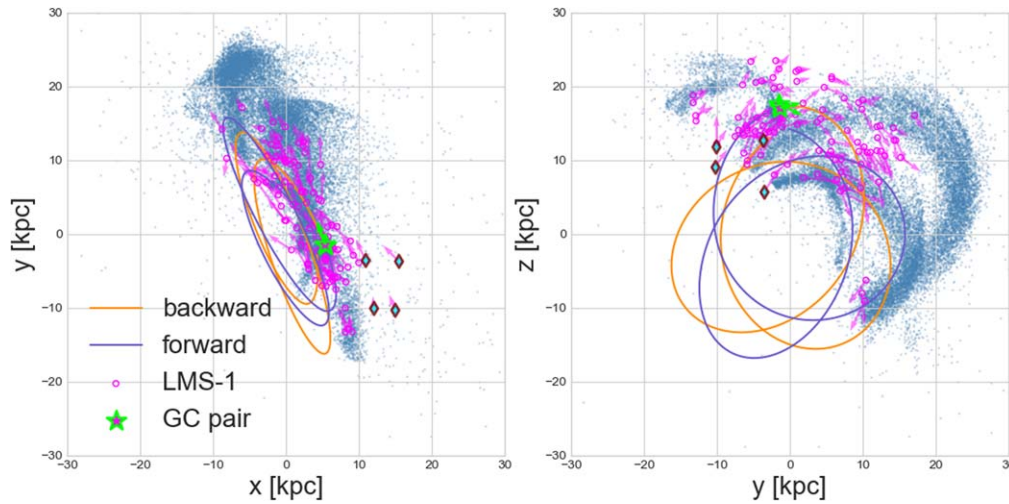


Figure 4. LMS-1, with the pair of GCs, and the simulated stream in the observable sky (decl. $> -10^\circ$) on the orbit of NGC 5024 with eight apocentric passages, in Galactocentric coordinates (x, y) and (y, z) , plotted in the same way as Figure 3. The arrow of each stream member indicates its velocity vector, which generally follows the trajectory of the stream at its location. The observed members are very likely a mixture of stellar debris from multiple wraps stripped at different epochs.

5. Conclusions

In this work, we employ two types of old stars, BHBs and RRLs, to construct a fair sample of ~ 7600 stars in the ancient halo. Both are excellent distance indicators, thus we are able to obtain accurate 6D kinematic information for this halo sample, and derive their dynamical parameters. We apply the neural-network-based clustering method STARGO to this sample in the space of orbital energy and angular momentum, and identify four DTGs that are confidently associated with known MW GCs. The largest group, DTG-2, is confirmed to be the Sgr stream, and the other two, DTG-1 and DTG-4, are very likely the debris of Seq and GES left in the outer halo.

We show that DTG-3 is a new stream, having a very polar orbit with inclination angle of 80° , which we refer to as LMS-1. It is associated with a pair of GCs (NGC 5024 and NGC 5053), which is the first example of a low-mass stellar-debris stream with embedded GCs from a disrupted low-mass dwarf galaxy. By tracing the orbit of the more massive member of the pair, NGC 5024, we suggest that it is probably the core of the dwarf galaxy progenitor of LMS-1 and NGC 5053. We then use the orbital information of NGC 5024 as the initial condition for a dwarf satellite with a total mass of $2 \times 10^9 M_\odot$, and run an N -body simulation in an analytic MW potential. The resulting stream nicely covers the observed LMS-1 in both hemispheres, with a few outliers possibly due to orbital precession.




The stellar system of LMS-1 and its pair of GCs belongs to the vast polar structure (VPOS; Riley & Strigari 2020), initially suggested by Pawlowski et al. (2012). Although recent studies have shown that the orbital poles of the existing stellar streams and GCs do not cluster around the direction of the VPOS, the LMS-1 system adds a substantial accreted dwarf to it. We believe that numerous additional low-mass stellar-debris streams remain to be discovered that could be associated with GCs in the outer halo. This will help build a more complete MW assembly history, as well as open a new window to study the formation and evolution of GCs in ancient dwarf galaxies.

This work has made use of data from the European Space Agency (ESA) mission Gaia (<https://www.cosmos.esa.int/gaia>), processed by the Gaia Data Processing and Analysis

Consortium (DPAC, <https://www.cosmos.esa.int/web/gaia/dpac/consortium>). Funding for the DPAC has been provided by national institutions, in particular the institutions participating in the Gaia Multilateral Agreement.

The authors would like to thank the referee for constructive comments. Z.Y. wishes to thank Eugene Vasiliev for insightful discussions about the GC pair, and Iulia Simion for sharing her expertise on VOD and HAC. Z.Y. acknowledges the support from the LAMOST Fellow project, and Shanghai Sailing Program (Y955051001). J.C. is supported by Young Scientists Foundation of JiangSu Province (BK20181110), the NSFC fundings (No. 11825303, 11861131006) and the Alibaba Cloud Fellowship. T. C.B. acknowledges partial support from grant PHY 14-30152, Physics Frontier Center/JINA Center for the Evolution of the Elements (JINA-CEE), awarded by the US National Science Foundation. T.C.B. is also grateful for support from a PIFI Distinguished Scientist award from the Chinese Academy of Sciences. Y.H. is supported by National Natural Science Foundation of China grants 11903027, 11973001, 11833006, 11811530289, U1731108, and U1531244, and National Key R&D Program of China No. 2019YFA0405503.

ORCID iDs

Zhen Yuan  <https://orcid.org/0000-0002-8129-5415>
 Timothy C. Beers  <https://orcid.org/0000-0003-4573-6233>
 Yang Huang  <https://orcid.org/0000-0003-3250-2876>

References

- Antoja, T., Ramos, P., Mateu, C., et al. 2020, *A&A*, **635**, L3
 Baumgardt, H. 2017, *MNRAS*, **464**, 2174
 Bellazzini, M., Ibata, R., Malhan, K., et al. 2020, *A&A*, **636**, A107
 Belokurov, V., Erkal, D., Evans, N. W., Koposov, S. E., & Deason, A. J. 2018, *MNRAS*, **478**, 611
 Belokurov, V., Evans, N. W., Bell, E. F., et al. 2007, *ApJL*, **657**, L89
 Boberg, O. M., Friel, E. D., & Vesperini, E. 2015, *ApJ*, **804**, 109
 Boberg, O. M., Friel, E. D., & Vesperini, E. 2016, *ApJ*, **824**, 5
 Chun, S.-H., Kim, J.-W., Sohn, S. T., et al. 2010, *AJ*, **139**, 606
 Deng, L.-C., Newberg, H. J., Liu, C., et al. 2012, *RAA*, **12**, 735
 Gaia Collaboration, Brown, A. G. A., Vallenari, A., et al. 2018, *A&A*, **616**, A1
 Georgiev, I. Y., Puzia, T. H., Goudfrooij, P., & Hilker, M. 2010, *MNRAS*, **406**, 1967

- Grillmair, C. J., & Dionatos, O. 2006, *ApJL*, **643**, L17
- Harris, W. E. 2010, arXiv:1012.3224
- Haywood, M., Di Matteo, P., Lehnert, M. D., et al. 2018, *ApJ*, **863**, 113
- Helmi, A., Babusiaux, C., Koppelman, H. H., et al. 2018, *Natur*, **563**, 85
- Helmi, A., & de Zeeuw, P. T. 2000, *MNRAS*, **319**, 657
- Huxor, A. P., Ferguson, A. M. N., Tanvir, N. R., et al. 2011, *MNRAS*, **414**, 770
- Ibata, R., Bellazzini, M., Thomas, G., et al. 2020, *ApJL*, **891**, L19
- Koppelman, H. H., Helmi, A., Massari, D., Price-Whelan, A. M., & Starkenburg, T. K. 2019, *A&A*, **631**, L9
- Law, D. R., & Majewski, S. R. 2010, *ApJ*, **718**, 1128
- Lee, Y. S., Beers, T. C., Sivarani, T., et al. 2008a, *AJ*, **136**, 2022
- Lee, Y. S., Beers, T. C., Sivarani, T., et al. 2008b, *AJ*, **136**, 2050
- Lindgren, L., Hernández, J., Bombrun, A., et al. 2018, *A&A*, **616**, A2
- Liu, G. C., Huang, Y., Zhang, H. W., et al. 2020, *ApJS*, **247**, 68
- Mackey, A. D., Ferguson, A. M. N., Huxor, A. P., et al. 2019, *MNRAS*, **484**, 1756
- Mackey, A. D., Huxor, A. P., Ferguson, A. M. N., et al. 2010, *ApJL*, **717**, L11
- Malhan, K., Ibata, R. A., Carlberg, R. G., et al. 2019, *ApJL*, **886**, L7
- Malhan, K., Ibata, R. A., & Martin, N. F. 2018, *MNRAS*, **481**, 3442
- Massari, D., Koppelman, H. H., & Helmi, A. 2019, *A&A*, **630**, L4
- Matsuno, T., Aoki, W., & Suda, T. 2019, *ApJL*, **874**, L35
- McMillan, P. J. 2017, *MNRAS*, **465**, 76
- Myeong, G. C., Evans, N. W., Belokurov, V., Sanders, J. L., & Koposov, S. E. 2018a, *ApJL*, **856**, L26
- Myeong, G. C., Evans, N. W., Belokurov, V., Sanders, J. L., & Koposov, S. E. 2018b, *MNRAS*, **478**, 5449
- Myeong, G. C., Vasiliev, E., Iorio, G., Evans, N. W., & Belokurov, V. 2019, *MNRAS*, **488**, 1235
- Naidu, R. P., Conroy, C., Bonaca, A., et al. 2020, arXiv:2006.08625
- Ngeow, C.-C., Belecki, J., Burruss, R., et al. 2020, *AJ*, **160**, 31
- Pawlowski, M. S., Pflamm-Altenburg, J., & Kroupa, P. 2012, *MNRAS*, **423**, 1109
- Price-Whelan, A. M., & Bonaca, A. 2018, *ApJL*, **863**, L20
- Ramos, P., Mateu, C., Antoja, T., et al. 2020, *A&A*, **638**, A104
- Riley, A. H., & Strigari, L. E. 2020, *MNRAS*, **494**, 983
- Simion, I. T., Belokurov, V., Irwin, M., & Koposov, S. E. 2014, *MNRAS*, **440**, 161
- Simion, I. T., Belokurov, V., & Koposov, S. E. 2019, *MNRAS*, **482**, 921
- Sohn, S. T., Watkins, L. L., Fardal, M. A., et al. 2018, *ApJ*, **862**, 52
- Vasiliev, E. 2019a, *MNRAS*, **484**, 2832
- Vasiliev, E. 2019b, *MNRAS*, **482**, 1525
- Xue, X.-X., Ma, Z., Rix, H.-W., et al. 2014, *ApJ*, **784**, 170
- Xue, X. X., Rix, H. W., Zhao, G., et al. 2008, *ApJ*, **684**, 1143
- Yanny, B., Rockosi, C., Newberg, H. J., et al. 2009, *AJ*, **137**, 4377
- Yuan, Z., Chang, J., Banerjee, P., et al. 2018, *ApJ*, **863**, 26
- Yuan, Z., Myeong, G. C., Beers, T. C., et al. 2020, *ApJ*, **891**, 39
- Yuan, Z., Smith, M. C., Xue, X.-X., et al. 2019, *ApJ*, **881**, 164
- Zhao, G., Zhao, Y.-H., Chu, Y.-Q., Jing, Y.-P., & Deng, L.-C. 2012, *RAA*, **12**, 723